



## RESEARCH ARTICLE

10.1029/2021JD036369

### Special Section:

The land-air coupling over Tibetan Plateau and its global climate effects

### Key Points:

- Leading variation in surface potential vorticity (PV) over the Tibetan Plateau (TP) is closely related to the TP's thermal and dynamic forcings during summer
- The North Atlantic tripole sea surface temperature (SST) mode could influence surface PV over the TP via Rossby wave, PV- $\theta$  mechanism, and local positive feedback
- The middle center in the tripole SST mode is critical in triggering the Rossby wave train affecting the TP

### Supporting Information:

Supporting Information may be found in the online version of this article.

### Correspondence to:

B. He and G. Wu,  
[heb@lasg.iap.ac.cn](mailto:heb@lasg.iap.ac.cn);  
[gxwu@lasg.iap.ac.cn](mailto:gxwu@lasg.iap.ac.cn)

### Citation:

Sheng, C., He, B., Wu, G., Liu, Y., Zhang, S., & Zhang, P. (2022). Interannual impact of the North Atlantic tripole SST mode on the surface potential vorticity over the Tibetan Plateau during boreal summer. *Journal of Geophysical Research: Atmospheres*, 127, e2021JD036369. <https://doi.org/10.1029/2021JD036369>

Received 17 DEC 2021

Accepted 20 APR 2022

© 2022. The Authors.

This is an open access article under the terms of the [Creative Commons Attribution-NonCommercial-NoDerivs License](https://creativecommons.org/licenses/by-nc-nd/4.0/), which permits use and distribution in any medium, provided the original work is properly cited, the use is non-commercial and no modifications or adaptations are made.

# Interannual Impact of the North Atlantic Tripole SST Mode on the Surface Potential Vorticity Over the Tibetan Plateau During Boreal Summer

Chen Sheng<sup>1,2</sup> , Bian He<sup>1,2</sup> , Guoxiong Wu<sup>1,2</sup>, Yimin Liu<sup>1,2</sup>, Shaoyu Zhang<sup>1,2</sup>, and Ping Zhang<sup>1,2</sup> 

<sup>1</sup>State Key Laboratory of Numerical Modeling for Atmospheric Sciences and Geophysical Fluid Dynamics (LASG), Institute of Atmospheric Physics, Chinese Academy of Sciences, Beijing, China, <sup>2</sup>College of Earth and Planetary Sciences, University of Chinese Academy of Sciences, Beijing, China

**Abstract** The Tibetan Plateau (TP) is an important forcing in the global climate system. Compared to the extensive studies on the influence of the TP on surrounding climates, the variability of the surface potential vorticity (PV) over the TP (TPSPV) in response to other forcings is seldom discussed. In this article, the influence of the interannual mode of North Atlantic tripole sea surface temperature (NAT) on the TPSPV during boreal summer is investigated. Results show that the negative (positive) anomalous TPSPV is associated with anomalous unstable (stable) surface air, cyclonic (anticyclonic) surface circulation, and rising (sinking) motion, which favors the stronger (weaker) East Asian summer monsoon and weaker (stronger) Indian summer monsoon. Further analysis indicates that the negative TPSPV is significantly correlated with a positive NAT mode with a cold center in the middle and warm centers in the subtropic and subpolar regions. This relationship is further testified by numerical experiments. The results further demonstrate that the positive NAT forcing can stimulate a Rossby wave train aloft, which passes Scandinavia, Ural and arrives at the TP and eventually triggers a low-level positive PV over the TP. Constrained by the PV- $\theta$  mechanism, the low-level positive PV favors a decrease in static stability near the surface and thus leads to a negative TPSPV. Under the positive feedback between TPSPV and vertical motion, the negative TPSPV could further strengthen. Therefore, the positive NAT phase could intensify the thermal and dynamic forcings of the TP in association with TPSPV during boreal summer.

## 1. Introduction

The enormous Tibetan Plateau (TP), rising proudly above tropical eastern Eurasia, plays a vital role in regional and global weather and climate by virtue of its mechanical and thermal effects (e.g., Flohn, 1957; Wu et al., 1997; Yanai et al., 1992; Ye & Gao, 1979; Ye et al., 1957). For example, studies have suggested that the air pump driven by sensible heating in the preceding spring (Duan et al., 2005; Zhao & Chen, 2001) and concurrent summer (He et al., 2015, 2019; Wu et al., 1997, 2007, 2012) prominently regulates the Asian summer climate pattern. Summer sensible heating and condensational heating over the TP could trigger a prominent potential vorticity (PV) forcing in the westerlies and therefore impact the downstream circulation via Rossby wave dispersion (Wu et al., 2016). In addition to the downstream climate, TP heating would exert a great impact on the upstream climate over West Asia, the Middle East, North Africa, and South Europe via zonal-vertical overturning circulation and wave train patterns (Lu et al., 2018, 2019; Nan et al., 2019). Besides the thermal forcing, the mechanical effect is also recognized as an important forcing in regulating the climate and weather (e.g., Bolin, 1950; Boos & Kuang, 2013; Charney & Eliassen, 1949; Chiang et al., 2020; Son et al., 2021). Numerical experiments illustrated that the uplifting TP pushed the edge of the South Asian summer monsoon northward (Chen et al., 1999; Jiang et al., 2008; Kitoh, 2004; Liu, 1999). The TP enable the establishment of the Atlantic Meridional Overturning Circulation (Fallah et al., 2016; Yang & Wen, 2020) and result in collapse of the Pacific Meridional Overturning Circulation (Wen & Yang, 2020). Theoretical and modeling studies suggested that the relative importance of the thermal and mechanical forcing, which is not the focus of this study, is very sensitive to the strength of the basic flow (Held & Ting, 1990; Held et al., 2002). Moreover, a latest study revealed that the monsoon responses to different heating regions of TP are quite different (Lu et al., 2021). Overall, the TP is an important mechanical and thermal forcing that adjusts the energy and hydrological cycle in the Earth system (Liu et al., 2020).

**Table 1**  
*List of Abbreviations Used in This Study*

Abbreviations	Full name
TP	Tibetan Plateau
PV	Potential Vorticity
TPSPV	Surface PV over the TP
PVNUM	EOF1 of TPSPV: surface PV Negative Uniform leading Mode
PVNUM1	PC1 corresponding to the PVNUM
NAT	EOF1 of North Atlantic SST: North Atlantic Tripole SST mode
NATI	PC1 corresponding to the NAT
NASUT	North Atlantic, Scandinavia, Ural and Western TP wave train

Given the influence of the TP, many studies have investigated the large-scale factors controlling the surface air temperature and precipitation of TP. In addition to tropical signals, including the Indian Ocean Basin Mode in May (Zhao et al., 2018), the winter and spring ENSO (e.g., Tao et al., 2011; Xu & Wang, 2016), and the decay speed of ENSO (Liang et al., 2021), an important extratropical factor is the North Atlantic tripole sea surface temperature (NAT) mode (e.g., Cui et al., 2015; Yu et al., 2021). Previous studies suggested that the NAT mode is coupled with North Atlantic Oscillation (NAO) during boreal winter and spring (e.g., Deser & Timlin, 1997; Li et al., 2019; Watanabe & Kimoto, 2000). However, this connection becomes weak during boreal summer (e.g., Yu, 2020). The summer NAT mode features the cold sea surface temperature (SST) center to the southeast of Newfoundland and the two warm SST centers in the tropical and subpolar North Atlantic, which is the interannual leading mode of empirical orthogonal function (EOF1) over the North Atlantic. Cui et al. (2015) suggested that the early spring (February–April) NAT could intensify the spring westerly jet over the TP. Yu et al. (2021) indicated that the March NAT could influence spring sensible heating over the TP. Some studies suggested that the spring NAT could influence the spring rainfall over southern China (Li et al., 2018) and subsequent summer rainfall over East Asia (e.g., Wu et al., 2009). The climate effect of NAT in winter and spring is the primary interest in the literature (e.g., Cui et al., 2015; Li et al., 2018; Li et al., 2019; Yu et al., 2021). However, research on the climate effects of NAT in summer when the thermal forcing of the TP peaks (Zhao et al., 2018) is still insufficient. Due to the seasonal shift in the basic flow from winter–spring to summer, it is unclear whether and how the NAT affects the TP during boreal summer. This issue remains open and needs to be further investigated.

The TP is a well-known forcing during boreal summer. To measure the changes in the TP's forcing, Sheng et al. (2022) indicated using the PV (Ertel, 1942; Rossby, 1940) framework at the TP surface could well depict both the mechanical and thermal changes in mountain forcing. Previous studies (e.g., Ma et al., 2019; Sheng et al., 2021; Yu et al., 2019; Zhang et al., 2021) revealed the significant influence of the TP surface PV (TPSPV) on the TP vortex, downstream extreme events, and East Asian general circulation and rainfall. However, how the TPSPV is controlled by other climate factors, especially the NAT mode of interest, remains unknown. Therefore, the present study aims to identify the interannual impact of the NAT mode on the TPSPV during boreal summer, which has received less attention in the previous literature. The outline for this study is given as follows. Section 2 documents the data, method, and model employed in this study. Section 3 presents the features of TPSPV and the associated local atmospheric thermal and dynamical structure. Section 4 investigates the interannual influence of the NAT mode on the TPSPV and analyses the possible mechanism. The summary and discussion are presented in Section 5.

For convenience, the abbreviations used in this study are listed in Table 1.

## 2. Data, Method, and Model

### 2.1. Data

Monthly mean data sets archived at the pressure level and hybrid  $\sigma$ – $p$  level, including zonal wind, meridional wind, vertical wind, air temperature, and pressure, are obtained from MERRA2 (Gelaro et al., 2017; Rienecker

et al., 2011). Monthly 2 m wind is obtained from the single level of MERRA2. Monthly mean SST data are obtained from the COBE SST data set (Ishii et al., 2005). Monthly land precipitation data are obtained from the Climatic Research Unit (Mitchell & Jones, 2005).

Three-hourly data archived at the hybrid  $\sigma$ - $p$  level obtained from MERRA2 are adopted to calculate the vertical PV flux ( $-\omega \cdot \text{PV}$ ).

The research period in this study is 1980–2017. The horizontal resolution of MERRA2 data is  $1.25^\circ \times 1.25^\circ$ . The horizontal resolutions of the precipitation data and SST data are  $0.5^\circ \times 0.5^\circ$  and  $1^\circ \times 1^\circ$ , respectively. Boreal summer refers to the time averaged over June–August (JJA).

The linear trend and the low-frequency variation (more than 9 years; using Lanczos filter, [http://www.ncl.ucar.edu/Document/Functions/Built-in/filwgtls\\_lanczos.shtml](http://www.ncl.ucar.edu/Document/Functions/Built-in/filwgtls_lanczos.shtml)) are filtered out in raw data to focus on the interannual variability. “\*\*\*” (“\*\*”) indicates a significance level exceeding 0.01 (0.05) unless otherwise specified.

## 2.2. Method

Following Sheng et al. (2021), surface PV is calculated as follows:

$$\text{PV} = g \left[ \frac{\partial v}{\partial p} \left( \frac{\partial \theta}{\partial x} \right)_h - \frac{\partial u}{\partial p} \left( \frac{\partial \theta}{\partial y} \right)_h \right] - g \left[ f + \left( \frac{\partial v}{\partial x} \right)_h - \left( \frac{\partial u}{\partial y} \right)_h \right] \frac{\partial \theta}{\partial p}, \quad (1)$$

where  $g$  is gravity and is equal to  $9.8 \text{ m s}^{-2}$ ,  $p$  indicates pressure,  $\theta$  indicates potential temperature,  $f$  indicates the Coriolis parameter,  $(u, v)$  indicates horizontal wind, and  $h$  indicates that the horizontal difference is executed at the hybrid  $\sigma$ - $p$  level. The surface PV is obtained from the two bottom levels at the hybrid  $\sigma$ - $p$  level.

The surface static stability is  $-\partial\theta/\partial p$ , in which  $\theta$  and  $p$  are archived at the two bottom hybrid  $\sigma$ - $p$  levels.

The Rossby wave activity flux (WAF) is used to track the pathway of the wave energy, which is obtained from Takaya and Nakamura (2001). The horizontal WAF is calculated as follows:

$$\text{WAF} = \frac{p}{2|U|} \left\{ \begin{array}{l} \bar{u} (\psi'^2_x - \psi' \psi'_{xx}) + \bar{v} (\psi'_{xy} \psi'_y - \psi' \psi'_{xy}) \\ \bar{u} (\psi'_{xy} \psi'_y - \psi' \psi'_{xy}) + \bar{v} (\psi'^2_y - \psi' \psi'_{yy}) \end{array} \right\}, \quad (2)$$

in which  $p$  indicates the pressure,  $|U|$  indicates the horizontal wind speed, and  $\psi$  denotes the geostrophic stream function. The subscript represents the partial derivative. The bar represents the time mean, while prime means the time anomaly.

## 2.3. Model

The Atmospheric General Circulation Model used in this study is the Community Atmospheric Model version 4.0 (CAM4, Neale et al., 2013). The horizontal resolution of CAM4 in this study is approximately  $1.25^\circ \times 1^\circ$  (longitude  $\times$  latitude). The number of vertical levels is 26 and extends from the surface to 3.5 hPa. More details can be seen at <http://www.cesm.ucar.edu/models/cesm1.2/>.

The simple linear baroclinic model (LBM; Watanabe & Kimoto, 2000; Watanabe et al., 1999) is also used. Since the LBM excludes the complicated feedback of circulation on diabatic heating, it is helpful to understand the monodirectional physical response regarding a specific diabatic heating anomaly. The LBM is vertically represented by 20  $\sigma$  levels and horizontally represented by spherical harmonics with a resolution of T42. The LBM is a time-integrated primitive equation model that is linearized by the climatic mean state. The climatic mean state is taken as summer climatology in this study. Because of the dissipation effects, the model takes approximately 14 days to reach a steady state. Therefore, the last 15 days in the 30-day integration are used for analysis.

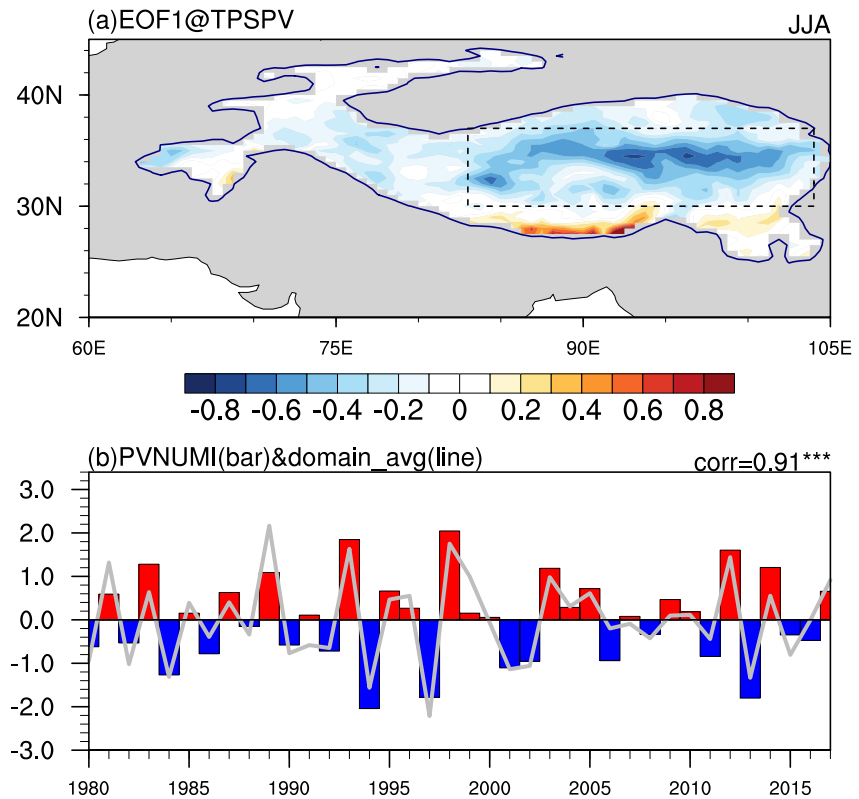


**Figure 1.** (a) The EOF1 mode of TPSPV with altitudes greater than 2,000 m during boreal summer. The blue line denotes the TP topographic boundary of 2,000 m. (b) The bar indicates the PVNUMI, which is PC1 corresponding to the EOF1 mode presented in (a). The gray curve indicates the domain-averaged TPSPV multiplied by  $(-1)$  with altitudes greater than 2,000 m.

### 3. The Interannual Features of TPSPV and Associated Circulations

#### 3.1. Dominant Mode of TPSPV

Figure 1a shows the EOF1 spatial pattern of TPSPV during boreal summer. It is clear that the horizontal distribution of variation in TPSPV features an almost overwhelming uniform negative sign that covers the TP platform. A positive sign with a small area only appears on the southern slope of the TP. In general, the variation in TPSPV shows a negative uniform mode (PVNUM), with the maximum variation occurring over the central-eastern TP. The explained variance in EOF1 is 36%. The leading principal component (PC1) corresponding to the PVNUM (Figure 1a) is denoted as the PVNUM index (PVNUMI) and shown as a bar in Figure 1b. In the positive PVNUM phase, the TPSPV is negative, and vice versa. It is evident that PVNUMI can well capture the features of domain-averaged TPSPV (multiplied by  $-1$  and shown as a gray line in Figure 1b), and the correlation coefficient is 0.91, passing the 0.01 significance level. This result confirms that the PVNUM is the dominant mode of the interannual variation in TPSPV.

Since the TPSPV couples the dynamic and thermal information, we linearly expand the variation in TPSPV to investigate which one that dominates and reveals the relevant atmospheric features. Because the TPSPV is largely determined by its vertical component (Sheng et al., 2021), the result of the linear expansion of TPSPV is described as follows:

$$\frac{\Delta PV}{A} \approx \underbrace{g(f + \zeta)}_B \Delta \left( -\frac{\partial \theta}{\partial p} \right) + \underbrace{g \Delta(f + \zeta)}_C \overline{\left( -\frac{\partial \theta}{\partial p} \right)} \quad (3)$$

in which  $\Delta$  indicates the time anomaly and the bar indicates the climate mean. This suggests that the variation in TPSPV is induced by both the variation in the static stability weighted by climatic absolute vorticity and the

variation in absolute vorticity weighted by climatic static stability; for convenience, we denote each term in Equation 3 in order as term A, term B and term C, respectively.

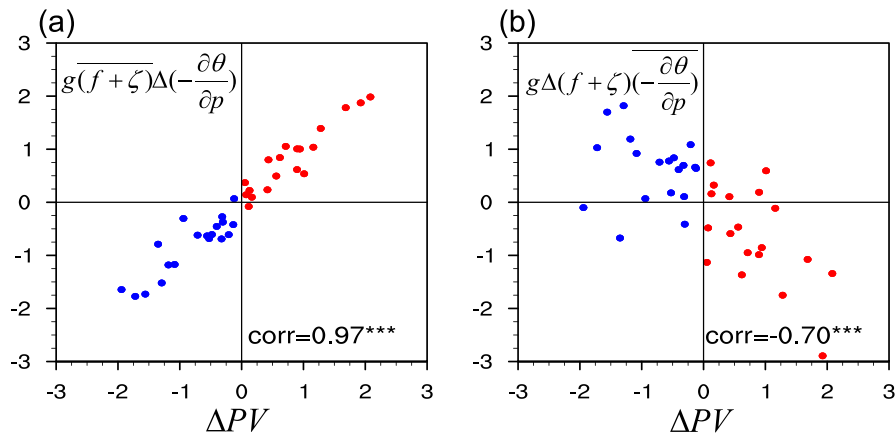
Figure 2a is the normalized scatter diagram showing the term A and term B averaged within the maximum variation region of TPSPV (dashed rectangle shown in Figure 1a). First, we calculate the raw standard deviation of each term in Equation 2, and the results in order are  $5.3 \times 10^{-2}$ ,  $6.3 \times 10^{-2}$ , and  $0.36 \times 10^{-2}$  PVU ( $1 \text{ PVU} = 10^{-6} \text{ K m}^2 \text{ kg}^{-1} \text{ s}^{-1}$ ). We can see that the standard deviation of term B is far larger than term C and is comparable with term A. From Figure 2a, we can further obtain that the variation in term B is in phase with the variation in term A, and the correlation coefficient is high at 0.97 and passes the 0.01 significance level. These results indicate that the variation in TPSPV (term A) is determined by the variation in surface static stability (term B). In other words, a negative (positive) anomalous TPSPV implies anomalous unstable surface (stable) air. Figure 2b is the same as Figure 2a but for term C. The correlation between term A and term C is as strong as  $-0.7$ , passing the 0.01 significance level, which means that the negative (positive) anomalous TPSPV implies anomalous cyclonic (anticyclonic) surface circulation. In brief summary, from Figures 2a and 2b, we argue that the negative (positive) anomalous TPSPV represents the underlying anomalous unstable (stable) surface air and anomalous cyclonic (anticyclonic) surface circulation. Furthermore, one can infer that such a configuration, with anomalous surface unstable (stable) air and anomalous cyclonic (anticyclonic) circulation embedded in negative (positive) anomalous TPSPV, favors an anomalous vertical rising (sinking) motion.

Figure 2c shows in hybrid  $\sigma$ - $p$  coordinate system the regression of the vertical profile of PV (green line), vertical pressure velocity multiplied by  $(-1; -\omega)$  (blue line), and vertical PV flux  $(-\omega \cdot \text{PV})$  (red line) averaged over the dashed rectangle in Figure 1a on the PVNUMI. The left labels indicate the pressure averaged over that dashed rectangle and the serial number of the hybrid  $\sigma$ - $p$  level. A novel vertical structure (green line) shows that the negative anomalous PV is only concentrated in a surface thin layer, while a deep positive anomalous PV column appears above this surface thin layer. The formation of such a vertical out-of-phase structure will be further addressed in Section 4.3. As predicted by Figures 2a and 2b, in the positive PVNUM phase, the anomalous rising motion (blue line, Figure 2c) is significant at the lower level. Owing to fluid continuity, this anomalous rising motion can even extend to the midupper level, which is in accord with Sheng et al. (2022). On the one hand, the underlying anomalous unstable surface air and anomalous cyclonic surface circulation embedded in PVNUM favor this anomalous rising motion. On the other hand, in return, the anomalous upward PV flux (red line) associated with the anomalous rising motion can reduce the surface PV and further strengthens the PVNUM. Consequently, PVNUM and anomalous rising motion are sustained via such positive feedback.

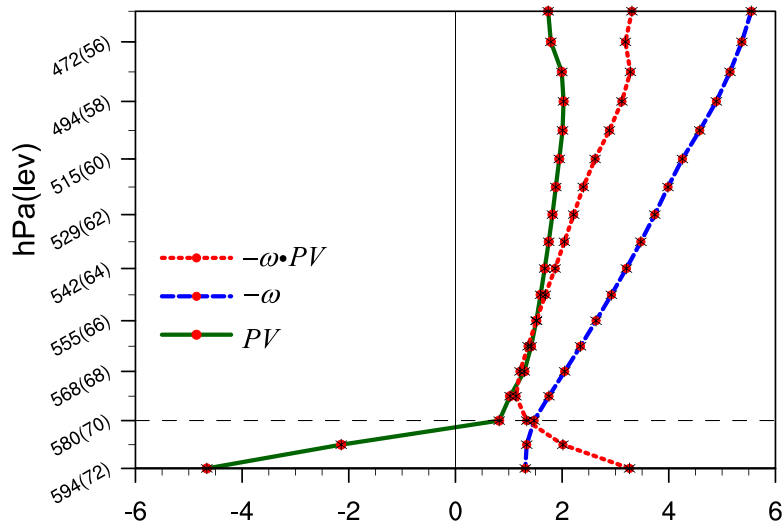
With reference to the schematic diagram showing the anomalous TPSPV (Figure 2d), we highlight such “PV thinking” again that the negative anomalous TPSPV is coupled with anomalous unstable surface air, anomalous cyclonic circulation, and anomalous rising motion. The positive anomalous TPSPV is coupled with anomalous stable surface air, anomalous anticyclonic circulation, and anomalous sinking motion. Notably, there is positive feedback between TPSPV and vertical PV flux, which is in favor of sustaining the configuration of negative (positive) anomalous TPSPV and anomalous rising (sinking) motion.

### 3.2. The Regional Circulation Associated With PVNUM

Following the “PV thinking” shown in Figure 2d, the relationship between TPSPV and Asian summer monsoon anomalies is intuitive. Figure 3a shows the correlation coefficients between PVNUMI and the Asian summer monsoon, including rainfall (shading) and near-surface (2 m) wind fields (vectors). The positive PVNUM phase, which is attributed to anomalous unstable surface air, anomalous cyclonic surface circulation, and anomalous rising motion over the TP (Figure 2d), favors changes in regional circulation and rainfall (Figure 3a). The air flow pumped by the TP, originating from the Pacific and passing the Bay of Bengal, converges into the eastern TP and results in more rainfall there (Figure 3a). For the South Asian region, the wet easterlies favor more rainfall over southern India. The northerlies in the western part of the surface cyclone near the TP lead to less rainfall over northern India. The divergence, which is attributed to the southerlies in the eastern part of the surface cyclone and lower-latitude easterlies, is responsible for the reduced rainfall over central India. For the East Asian region, the convergence leads to more rainfall over the Yangtze River valley, Korea, and Japan. The divergence of water vapor flux leads to less rainfall over southern China (Sheng et al., 2022). In general (Figure 3a), it is clear that the positive PVNUM phase corresponds to the strong East Asian summer monsoon and weak Indian summer monsoon.



(c) Regressed on PVNUMI



(d) Anomalous TPSPV

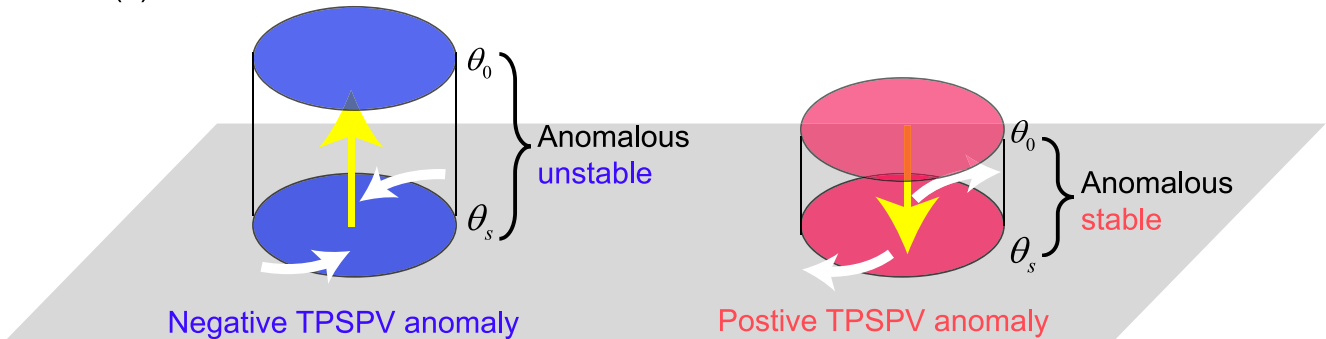


**Figure 2.** (a) Normalized scatter diagram showing the term A and term B in Equation 3 averaged within the dashed rectangle shown in Figure 1a. (b) Same as in (a) but for term C in Equation 3. (c) Regression of the vertical profile of PV (green line; units:  $10^{-2}$  PVU, 1 PVU =  $10^{-6}$  K m<sup>2</sup> kg<sup>-1</sup> s<sup>-1</sup>), vertical pressure velocity multiplied by (-1) ( $-\omega$ ; blue line; units:  $10^{-3}$  Pa s<sup>-1</sup>), and vertical PV flux ( $-\omega \cdot PV$ ; red line; units:  $10^{-3}$  PVU Pa s<sup>-1</sup>) averaged over the dashed rectangle in Figure 1a on the PVNUMI. The left labels in (c) indicate the averaged pressure over that dashed rectangle and the serial number of the hybrid  $\sigma$ - $p$  level. The red dot with an asterisk indicates exceeding 0.05 significance level. (d) Schematic diagram showing the anomalous TPSPV and the relevant circulation. The vectors indicate the 3-D winds within the surface layer.  $\theta_0$  and  $\theta_s$  indicate a given isentropic surface and the Earth's surface potential temperature, respectively.

Such an out-of-phase relationship between the Indian and East Asian summer monsoons implied by Figure 3a is clear in Figure 3b. The correlation coefficients between the PVNUMI and Indian summer monsoon index (Wang et al., 2001) and East Asian summer monsoon index (Zhao et al., 2015) yield  $-0.37$  (exceeding 0.05) and  $0.57$  (exceeding 0.01), respectively. This robust out-of-phase variation has been revealed in many previous studies

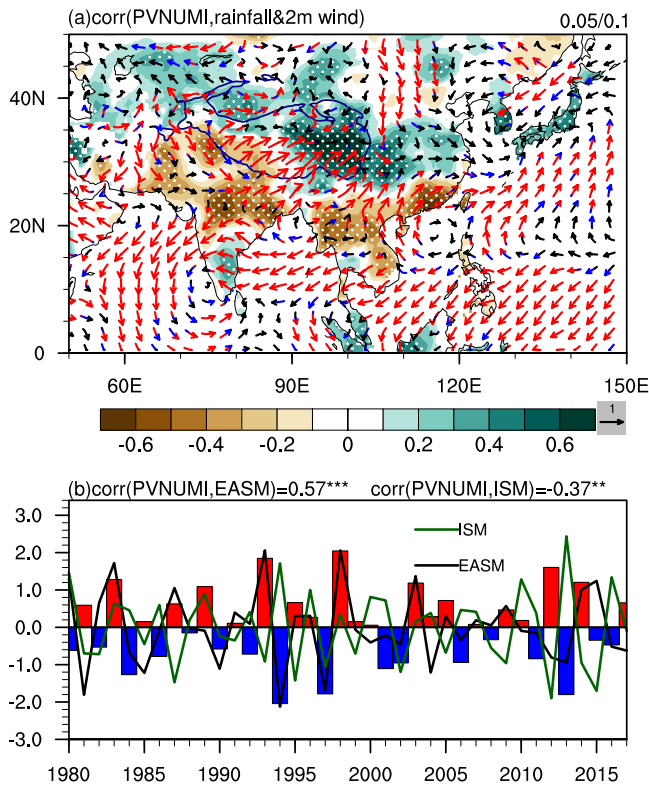


**Figure 3.** (a) Correlation coefficients between PVNUMI and rainfall (shading) and 2 m wind (vector) during boreal summer. Areas exceeding the 0.05 significance level are highlighted by white dots. Vectors exceeding the 0.05 (0.1) significance level are colored red (blue). The blue line denotes the TP topographic boundary of 3,000 m. (b) PVNUMI (bar), Indian summer monsoon index (green line), and East Asian summer monsoon index (black line).

(e.g., Kim et al., 2002; Kripalani & Kulkarni, 2001; Krishnan & Sugi, 2001; Wu, 2002, 2017). Here, we speculate that the TPSPV may play a role in connecting the out-of-phase variation between the Indian summer monsoon and East Asian summer monsoon and deserves further study.

#### 4. Interannual Influence of North Atlantic Tripole SST on the TPSPV and the Possible Mechanism

The previous section revisited the dominant mode of TPSPV and presented some fundamental features, including the TP's atmospheric thermal and dynamic structure associated with TPSPV and the potential role of TPSPV in the Asian summer monsoon change. In this section, we turn our attention to show the influence of the NAT mode of interest on the TPSPV during boreal summer through statistical analysis and numerical simulation studies.

##### 4.1. Data Diagnosis

Figure 4a shows the correlation between PVNUMI and SST over the North Atlantic. A positive NAT (Figure 4a) mode, with a positive anomalous SST to the tropical and subpolar North Atlantic and a negative anomalous SST to the south of Newfoundland, is significant. This NAT mode bears a marked resemblance to the EOF1 of the SST shown in Figure 4b. The explained variance of EOF1 is 24%. PC1 corresponding to Figure 4b is denoted as NATI to represent the NAT mode forcing, as shown in Figure 4c (green line). The correlation coefficient (Figure 4c) between PVNUMI and NATI is as strong as 0.44, exceeding the 0.01 significance level. These results indicate that the PVNUMI is related to the NAT mode during boreal summer. In the positive NAT phase, the PVNUMI is often in the positive phase, and the TPSPV is often negative, and vice versa.

The NAT mode can impact atmospheric circulation through the thermal wind constraint. The correlations between NATI and SST (Figure 5a) and atmospheric temperature (Figures 5b–5d) are presented in Figure 5. The distribution of atmospheric temperature (Figure 5b) closely resembles the SST pattern (Figure 5a), suggesting a prominent thermal impact of the NAT mode on the atmosphere. Due to the viscosity, the no-slip boundary condition illustrates that the velocity is very close to zero at the exact Earth's surface (Holton, 2004). Therefore, the thermal wind constraint can be approximated as

$$\vec{V}(p) = -\frac{R}{f} \int_{ps}^p (\vec{k} \times \nabla T) d \ln p, \quad (4)$$

in which  $\nabla$  is horizontal gradient operator,  $R$  indicates the gas constant,  $\vec{k}$  is the upward unit vector,  $ps$  is the Earth's surface pressure, and  $\vec{V}(p)$  is the horizontal wind at a certain pressure level. Subject to the thermal wind constraint (Equation 4), significant near-surface westerlies appear between the central cold SST center and southern warm SST center, and over the poleward side of the northern warm SST center, whereas significant near-surface easterlies appear between the central cold SST center and northern warm SST center (Figure 5a). Therefore, an anticyclone and cyclone (Figure 5a) are forced over the central and subpolar North Atlantic, respectively. From the low level (Figure 5b) to the upper level (Figure 5d), because the signs of temperature gradient over the central and subpolar North Atlantic remain unchanged, the near-surface circulation can be maintained and intensified with height (Equation 4). As a result, these circulation anomalies with an equivalent barotropic structure in response to NAT forcing can extend from the lower level (Figure 5b) to the midupper troposphere (Figures 5c and 5d).

To examine the mechanism linking the NAT mode and TP, the geopotential height (contour) and WAF (vectors) at 500 hPa regressed on the NATI are shown in Figure 6a. Figure 6a presents a prominent Rossby wave train extending from the North Atlantic to East Asia. It is also clear at 200 hPa (Figure S1 in Supporting Information S1),

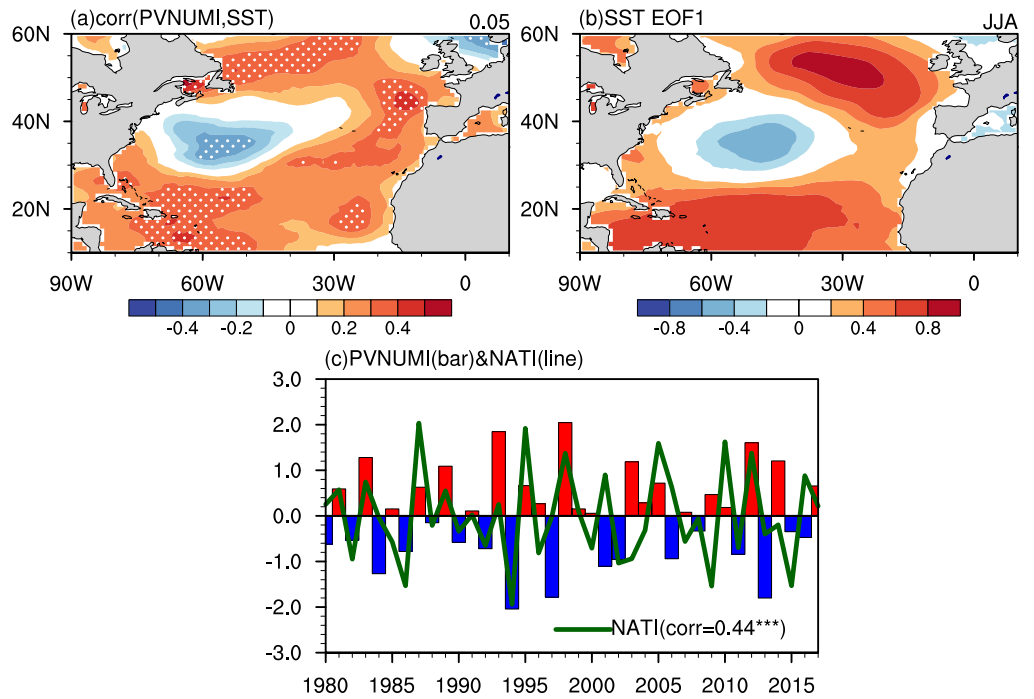


**Figure 4.** (a) Correlation coefficients between PVNUMI and SST over the North Atlantic during boreal summer. Areas exceeding the 0.05 significance level are highlighted by white dots. (b) EOF1 of the North Atlantic SST. (c) Time series of PVNUMI (bar) and NATI (line, PC1 corresponding to b).

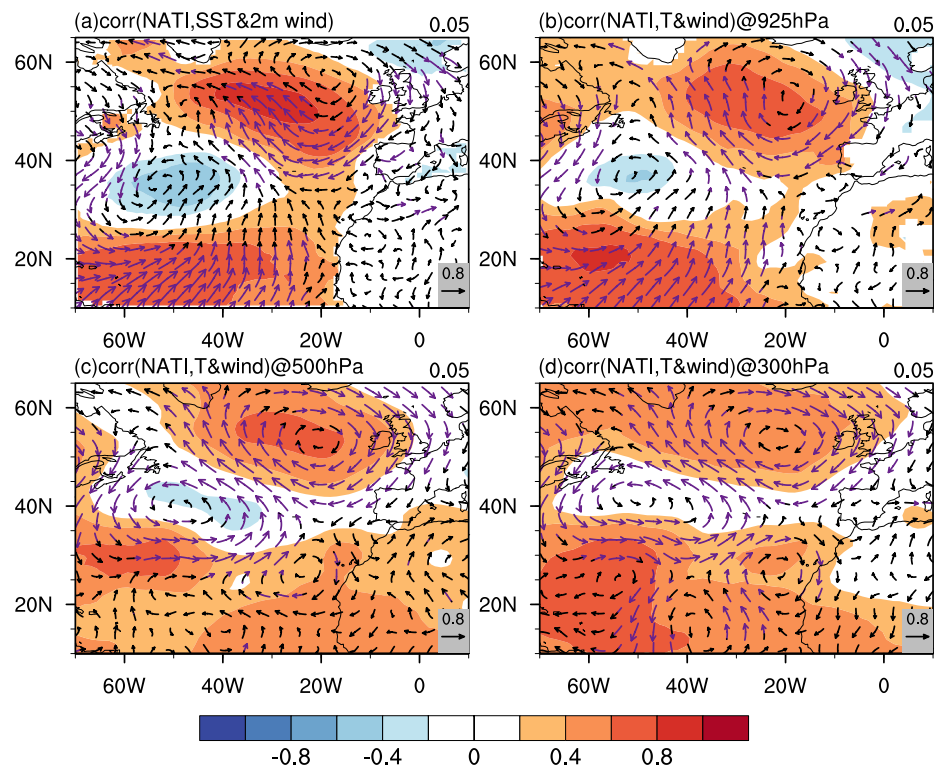


**Figure 5.** (a) Correlation coefficients between NATI and SST (shading) and 2 m wind (vectors) during boreal summer. Vectors exceeding the 0.05 significance level are colored purple; (b) same as in (a) but for air temperature and wind at 925 hPa; (c) same as in (b) but for 500 hPa; and (d) same as in (b) but for 300 hPa.

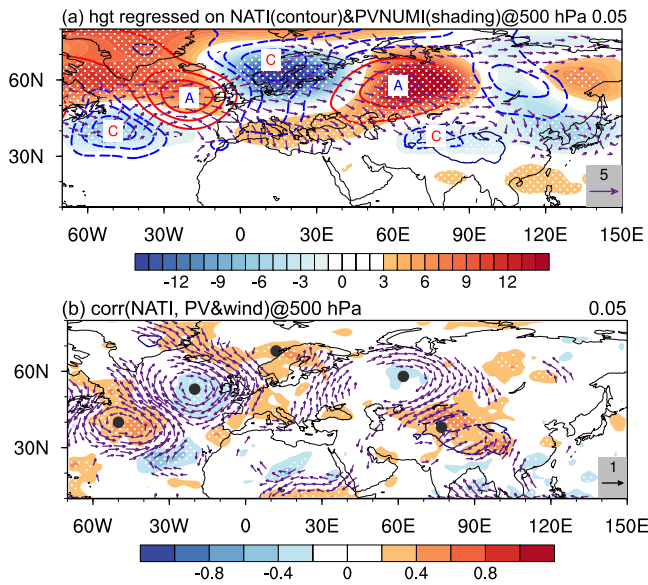


**Figure 6.** (a) Regression of geopotential height (units: gpm) on NATI (contour) and PVNUMI (shading) at 500 hPa during boreal summer. Vectors indicate the wave activity flux (units:  $\text{m}^2 \text{s}^{-2}$ ) regressed on NATI. (b) Correlation coefficients between NATI and PV (shading) and horizontal wind (vectors) at 500 hPa. Areas exceeding the 0.05 significance level are highlighted by white dots. The blue line denotes the TP topographic boundary of 3,000 m.

suggesting an equivalent barotropic structure. This wave train has five centers, located in the central and subpolar North Atlantic, Scandinavia, Ural, and western TP. This wave train is hereafter referred to as the NASUT wave train. By conducting the WAF analysis, the wave energy embedded in NASUT originates from the region above the central cold SST center in NAT mode and disperses downstream to the western TP. The regressed geopotential height (contour) on NATI bears great resemblance to that regressed on PVNUMI (shading), further confirming the close linkage between the NAT mode and PVNUMI. Figure 6b presents the correlation coefficients between NATI and PV (shading) and horizontal wind (vectors) at 500 hPa. The PV and horizontal wind fields embedded in the NASUT wave train are well organized. The positive PV accompanied by cyclonic circulation and the negative PV accompanied by anticyclonic circulation are arranged alternately downstream along the wave energy path. Consequently, a significant positive 500-hPa PV and cyclonic circulation are triggered over the TP. The above results indicate that the NASUT wave train plays a critical role in connecting the NAT mode and 500-hPa circulation over the TP.

#### 4.2. Numerical Experiments

Through Atmospheric General Circulation Model experiments based on CAM4, this section further verifies the aforementioned process. The control experiment is driven by the prescribed climatological annual cycle SST. Positive and negative NAT anomalies based on  $\text{NATI} > 1.0$  and  $\text{NATI} < -1.0$  are imposed onto the climatological SST, and we refer to these as positive (POS) and negative (NEG) experiments, respectively. For both experiments, the model was run in 20 members, and the last 15 members were analyzed.

More details of the experimental design are stated in Table 2. The SST forcing pattern can be found in Figure S2 in Supporting Information S1.

Figure 7a presents the composite differences in geopotential height and WAF between POS and NEG experiment ensemble means. Actually, there are some differences between model simulation (Figure 7) and reanalysis (Figure 6). Compared with reanalysis (Figure 6a), the main differences feature that the wave in model simulation (Figure 7a) could propagate well in the relative lower latitude ( $30^\circ$ – $50^\circ\text{N}$ ; Figure 7a), and the meridional scale of wave train (Figure 7a) is larger. This is mainly because the systemic wind bias of model (Figure S3 in Supporting Information S1). The model shows the westerly bias over the relative lower latitude (black line in Figure S3 in Supporting Information S1) and higher latitude (red line in Figure S3 in Supporting Information S1), and the easterly bias over the middle region (blue line in Figure S3 in Supporting Information S1). Due to the waveguide effect of westerly (Hoskins & Ambrizzi, 1993), the wave could propagate well in the relative lower latitude (Figure 7a). For the same reason, the wave could also go into the relative higher latitude (Figure 7a) and be trapped over there, leading to the larger meridional scale of the simulated wave. Since the numbers of original vertical level in MERRA2 and CAM4 are 72 and 26, respectively, the somewhat chaotic PV shown in Figure 7b

**Table 2**  
Experimental Design

Case	Description
Control	Atmospheric General Circulation Model run using the monthly mean climatological SSTs as the lower boundary conditions. The other forcing fields were prescribed as their climatological values. The experiment was integrated for 20 years.
POS	Climatological SSTs plus prescribed positive NAT mode. The simulation of 20 members integrated from 1 April to 30 September with the initial field taken from every 1 April of each year of the Control experiment. Considering stability, the forcing was set from 1 May to 31 August. The mean values over June–August of the last 15 members were analyzed.
NEG	Same as POS but forced by the prescribed negative NAT mode.

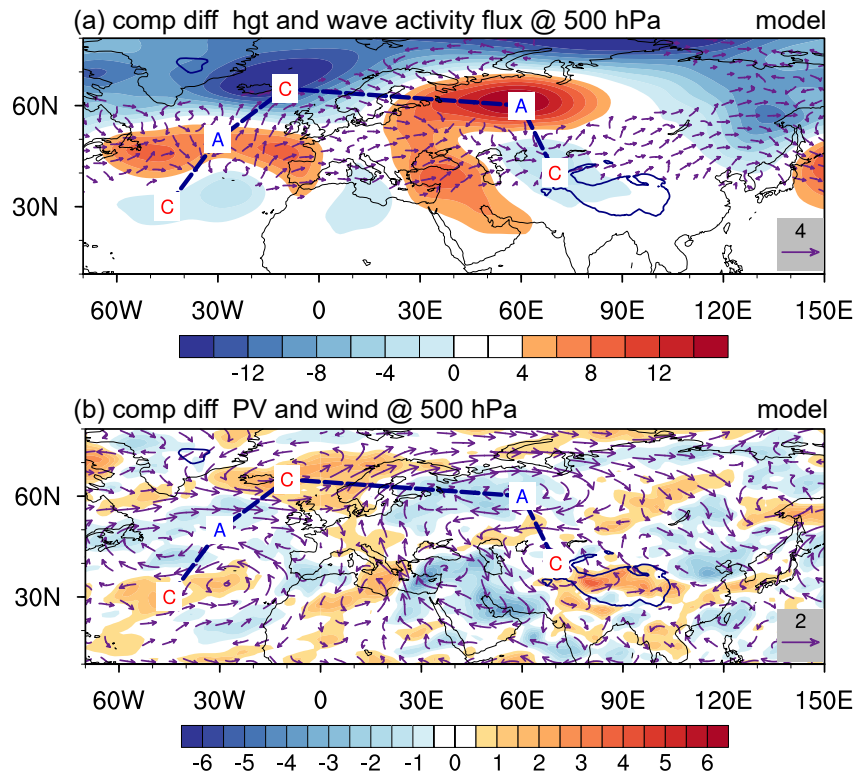


**Figure 7.** Differences between the POS and NEG ensemble means during boreal summer. (a) Geopotential height (shading; units: gpm) and wave activity flux (vectors; units:  $\text{m}^2 \text{s}^{-2}$ ) at 500 hPa. (b) PV (units:  $10^{-2}$  PVU) and horizontal winds (units:  $\text{m s}^{-1}$ ) at 500 hPa. The blue line denotes the TP topographic boundary of 3,000 m.

may result from a coarse original vertical resolution of the CAM4 model. Despite these differences, the NASUT wave train is generally well simulated. A wave train with five centers (Figure 7a), located in the central and subpolar North Atlantic, west of Scandinavia, Ural, and western TP, is very similar to a realistic NASUT wave train (Figure 6a). The WAF originating from the central North Atlantic, passing the Ural, reaches at the western TP is also clear. Along the WAF, the wave train with alternating signs in PV and horizontal winds (Figure 7b), which features positive PV and associated cyclonic circulation over the TP, resembles that in the reanalysis (Figure 6b). These results support that the NAT mode can stimulate the NASUT wave train and affect the 500-hPa circulation over the TP.

Notably, both the reanalysis (Figure 6a) and model (Figure 7a) imply that the wave energy may originate from the central North Atlantic. To further elucidate which anomalous SST center dominates generation of the NASUT wave train, we conducted three experiments by using the LBM. This simple model excludes the complicated feedback of circulation on diabatic heating and is helpful to examine the impact of anomalous diabatic heating on atmosphere. According to the reanalysis, the center (Figure 8a) of the northern warming, central cooling, and southern warming is located at  $60^\circ\text{W}$ ,  $51.5^\circ\text{N}$ ,  $50^\circ\text{W}$ ,  $35^\circ\text{N}$ , and  $45^\circ\text{W}$ ,  $17.5^\circ\text{N}$ , respectively. Each center has a prescribed ideal elliptic distribution with a maximum heating rate of 2 K/day (Figure 8b) to mimic the direct thermal forcing of the typical NAT mode (Cui et al., 2015).

We examine the 500-hPa response regarding each single diabatic forcing center (Figure 9) separately. In Figure 9, the contours of zonal wind speeds of 10 and 5 m/s are colored green and light blue, respectively. The zonal westerly jet core (green line, Figure 9) is located in the North Atlantic, and the stronger westerlies (light blue line) split into northern and southern branches over Eurasia.

In the experiment with only the northern warming center (Figure 9a), the strongest response appears to the exit region of the westerly jet core (green line) and disperses downstream along the stronger westerlies. The response in the northern branch reaches the area north of Lake Baikal, while that in the southern branch reaches the area east of the Caspian Sea.

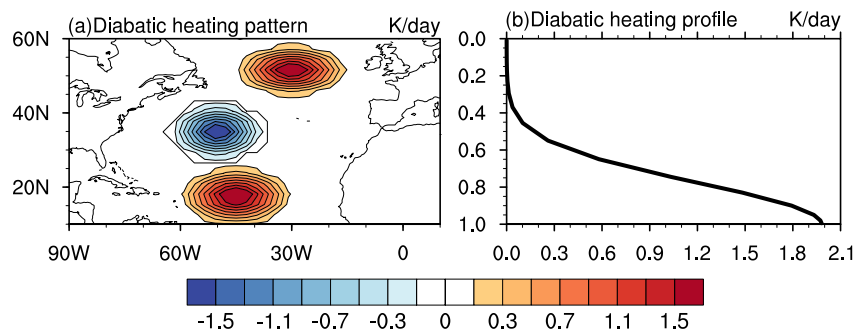


**Figure 8.** (a) Horizontal distribution of specified ideal diabatic heating. (b) Specified ideal diabatic heating profile (units: K/day).

In the experiment with only the central cooling center (Figure 9b), the strongest anomalous low response appears to the relative entrance region of the westerly jet core (green line), passes through the jet core, and propagates well along the stronger westerlies. Finally, one along the northern branch reaches Eastern Russia, and the other shifts

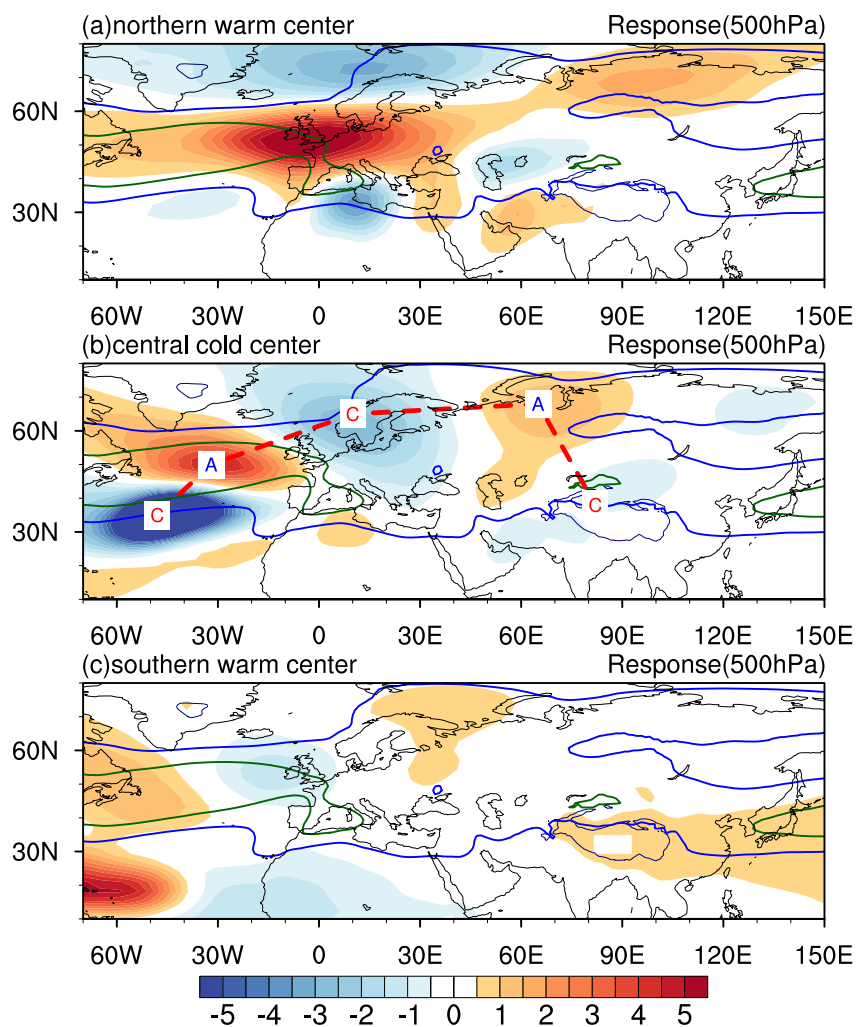


**Figure 9.** Response of boreal summer 500-hPa geopotential height (units: gpm) to the (a) northern warm SST only, (b) central cold SST only, and (c) southern warm SST only. The blue and green lines indicate zonal wind speeds equal to 5 and 10 m/s, respectively.

to the southern branch and arrives at the western TP. This wave pattern, extending from the North Atlantic to the western TP, is very similar to the NASUT wave train in reanalysis (Figure 6a).

In the experiment with only the southern warming center (Figure 9c), because the warming center is far away from the westerly jet core (green line), the generated wave energy is relatively weak in the stronger westerlies. It cannot propagate far downstream and rapidly dampens over eastern Scandinavia.

Comparing the response in the three experiments suggests that the 500-hPa circulation in response to the central cooling center closely resembles the realistic NASUT wave train, indicating that the central cold SST is critical for the generation of the NASUT wave train during boreal summer. This is mainly because the central cold SST and its thermal gradient are on the optimal location where is the relative entrance region of the westerly jet. Whereas the southern warming center is far away from the jet and the northern warming center is on the exit region of jet core, the two centers are thus only able to play a secondary role in the generation of NASUT wave train.

### 4.3. Formation of the Vertical Structure With Opposite Signs in PV Over the TP

Previous results confirm that the NAT mode could affect the 500-hPa circulation over the TP by stimulating the NASUT wave train. Significantly, in both the reanalysis (Figure 6b) and numerical experiments (Figure 7b), the positive NAT mode favors 500-hPa positive PV over the TP. However, the NAT mode is in phase with PVNUM (Figure 4c), which means that the positive NAT mode corresponds to the negative TPSPV. This finding suggests that from the surface to 500 hPa, there should be a vertical structure with opposite signs in the PV.

Figure 10a presents a cross section of correlation coefficients between the NATI and the 30°–37°N mean PV (shading) and static stability (contour) in the hybrid  $\sigma$ - $p$  level in the MERRA2 reanalysis. In the positive NAT phase (Figure 10a), it is evident that within a thin surface layer, there is a negative PV, whereas the positive PV is above it. Recalling the PV- $\theta$  mechanism (Hoskins et al., 2003; Hoskins, 1991; Hoskins et al., 1985; Figure S4 in Supporting Information S1), this vertical structure with opposite signs in PV becomes natural. According to the PV- $\theta$  mechanism (Figure S4 in Supporting Information S1), the isolated positive PV anomaly in the free atmosphere will vertically suck the isentropes and lead to the isentropes bowing downward (upward) in the space above (below) the positive PV anomaly. As the isentropes bow upward below the positive PV anomaly, the thickness between two isentropes increases, thus leading to a decrease in static stability at the lower level. In Figure 10a, with the downward intrusion of 500-hPa PV over the TP, owing to the PV- $\theta$  mechanism, the static stability near the surface layer decreases (dashed contour). Because the TPSPV is nearly determined by the static stability (Figure 2a), a negative TPSPV is formed. In the negative NAT phase, the situation is on the opposite.

Figure 10b is the same as Figure 2c but for the regression on NATI. In the positive NAT phase, the decrease in static stability associated with the negative PV near the surface layer favors the rising motion (blue line) over the TP. In return, the upward PV flux (red line) associated with rising motion further favors the reduction in TPSPV. This positive feedback has been documented in Figure 2c. Consequently, a negative TPSPV and rising motion are sustained. In addition, the PV, vertical motion, and vertical PV flux regressed on the NATI (Figure 10b) are half magnitude of typical variation of those variables (Figure 2c), indicating that the NAT can explain half of the anomalies of variation in the TPSPV and associated circulation.

In summary, in the positive NAT phase, governed by the PV- $\theta$  mechanism, and the positive feedback between TPSPV and vertical motion, the negative anomalous TPSPV within a surface thin layer below the positive anomalous PV embedded in the NASUT is retained (Figure 10c). The situation in the negative NAT phase is on the opposite.

## 5. Summary and Discussion

### 5.1. Summary

The TP is an important thermal and mechanical forcing during boreal summer. Compared to the numerous studies on the influence of TP on the weather and climate, the TPSPV in response to other forcings has received relatively less attention. Previous studies suggested that the NAT mode, an important extratropical factor, has a great impact

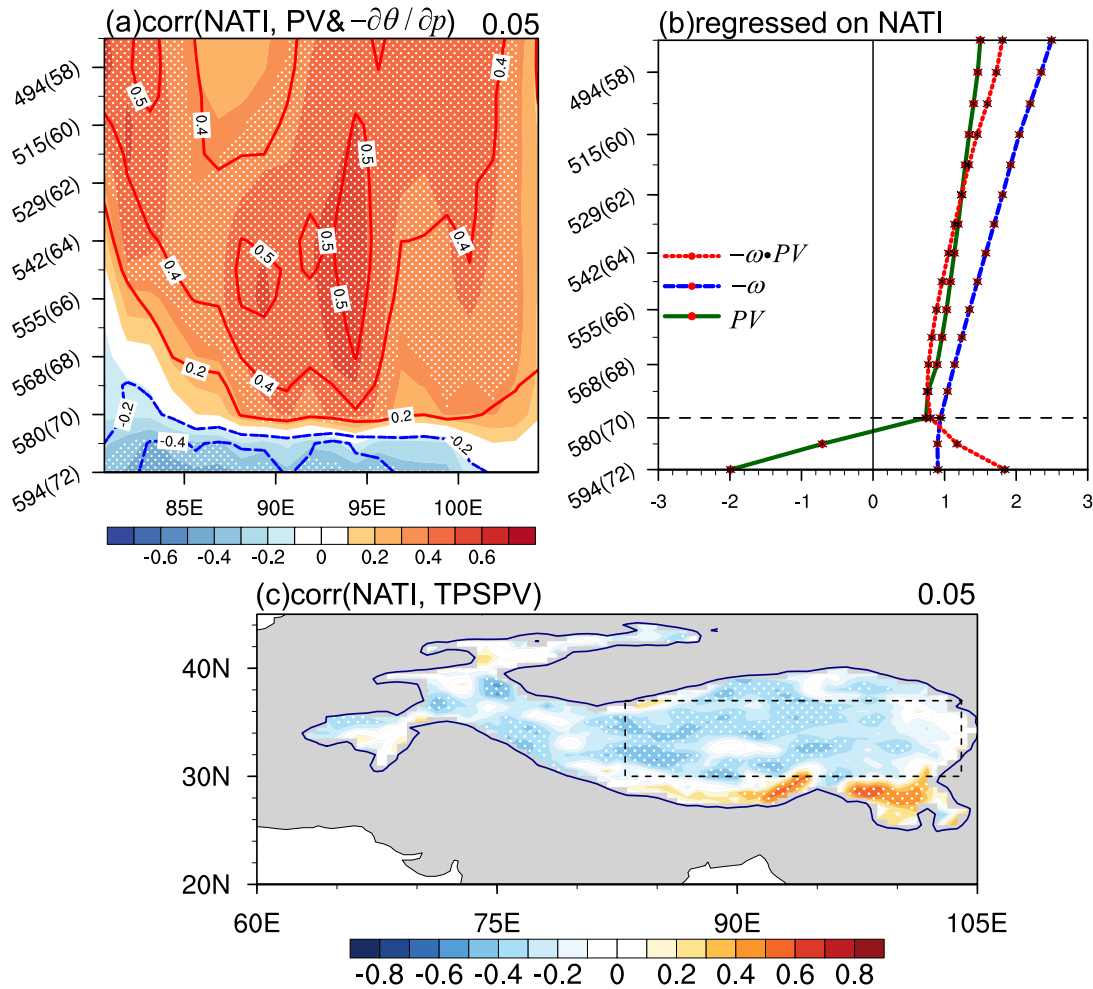


**Figure 10.** (a) Distribution of correlation coefficients between the NATI and the  $30^{\circ}$ – $37^{\circ}$ N mean PV (shading) and static stability (contour) in the hybrid  $\sigma$ - $p$  coordinate system during boreal summer. (b) Same as in Figure 2c, but for NATI. (c) Same as in Figure 1a but for correlation coefficients between NATI and TPSPV. Areas exceeding the 0.05 significance level are highlighted by white dots. The blue line denotes the TP topographic boundary of 2,000 m.

on the weather and climate downstream during boreal spring and winter, while the climate effects of NAT mode during boreal summer when the TP's forcing peaks are seldom discussed.

The TPSPV is a good indicator for capturing the TP's forcing (Ma et al., 2019; Sheng et al., 2021; Yu et al., 2019; Zhang et al., 2021). By using reanalysis and model simulation, the present study investigated the interannual impact of the NAT mode on the TPSPV during boreal summer. The major mechanism is shown as a schematic in Figure 11. The main conclusions obtained from the present study are summarized as follows:

1. The PVNUM, which features uniform negative TPSPV anomalies, is the leading mode of the interannual variation in TPSPV. The positive (negative) PVNUM phase corresponds to anomalous unstable (stable) surface air, anomalous cyclonic (anticyclonic) circulation, and anomalous rising (sinking) motion. Further analysis indicated that the TP's forcing related to the positive (negative) PVNUM phase favor the strong (weak) East Asian summer monsoon and weak (strong) Indian monsoon.
2. The NAT mode is the leading mode of SST over the North Atlantic on an interannual timescale. The positive NAT mode (Figure 11b) can lead to a significant anomalous local circulation aloft through the atmospheric thermal wind constraint and then stimulate a NAUST wave train downstream. The NAUST wave train originating from the North Atlantic, passing Scandinavia and Ural, reaches the TP and eventually triggers a cyclone and positive PV at low level (500 hPa; Figure 11a).

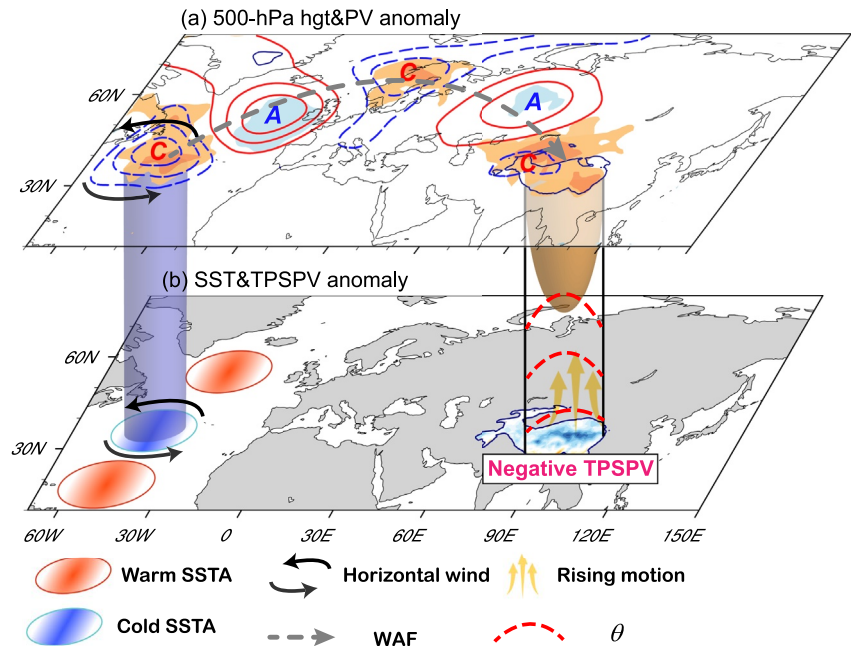


**Figure 11.** Schematic showing how the interannual NAT mode influences the TPSPV in boreal summer. (a) Geopotential height anomaly (contour) and PV anomaly (shading) at 500 hPa. (b) SST anomaly (SSTA) and TPSPV anomaly. The blue cylinder on the left indicates atmospheric cooling. The brown cone-like shape on the right indicates the positive PV downward intrusion. The blue line denotes the TP topographic boundary of 3,000 m.

3. The PV- $\theta$  mechanism (Figure S4 in Supporting Information S1) and a positive feedback process between the TPSPV and vertical motion are responsible for the TPSPV anomaly. The 500-hPa positive PV with downward intrusion (brown cone-like shape on right side of Figure 11) over the TP can directly lead to the negative anomalous TPSPV by reducing the static stability (bowing upward dashed red line on right side of Figure 11), while the decreased static stability can enhance the rising motion (yellow vectors on right side of Figure 11). In return, the anomalous upward PV flux associated with the anomalous rising motion can further lead to the reduction in TPSPV and strengthen the negative TPSPV (Figure 11b). Consequently, the NAT mode exerts a significant impact on the TPSPV via the NASUT wave train, PV- $\theta$  mechanism, and positive feedback between the TPSPV and vertical motion (Figure 11).
4. The LBM experiments further suggest that the middle center is critical in triggering the realistic NASUT wave train, because the middle center and its related thermal gradient are on the optimal location where is the relative entrance region of the westerly jet. However, the southern center is far away from the jet and the northern center is on the exit region of the jet core, and thus the two centers just play a secondary role in the formation of NASUT wave train.

## 5.2. Discussion

The winter and spring extratropical NAT mode (Cui et al., 2015; Yu et al., 2021) could affect the TP by triggering Rossby wave. However, because the basic flow in summer is different from that in winter and spring, it is not clear whether the NAT mode could affect the TP during boreal summer. This is a vital issue because the forcing of the TP peaks in summer, which will greatly influence the regional and global weather and climate. The present study confirms that the NAT mode can influence the TP during boreal summer. Compared with the Rossby wave train triggered by the NAT mode in winter–spring (see Figure 4d in Cui et al. [2015] and Figure 8a in Yu et al. [2021]), we found that although the Rossby wave train can arrive at the TP both in winter–spring and summer, their pathways and wave number are quite different. The different Rossby wave pathways will lead to different climate effects along the wave passing region. Therefore, the detailed reasons responsible for the different pathways deserve further investigation.

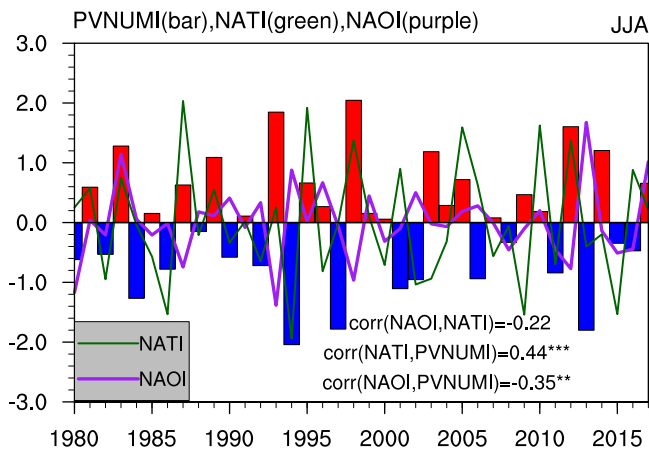


**Figure 12.** Time series of PVNUMI (bar), NATI (green line), NAOI (purple line), and their correlation coefficients during boreal summer.

Previous studies (e.g., Deser & Timlin, 1997; Li et al., 2019; Watanabe & Kimoto, 2000) suggested that the NAO and NAT are related to each other during boreal winter and spring. However, this intimate relation becomes weak during boreal summer (e.g., Yu, 2020). Figure 12 shows that the correlation between NAOI (NAO index; <https://psl.noaa.gov/data/correlation/nao.data>) and NATI drops to  $-0.22$ , which fails the significance test, meaning the summer NAO and NAT are statistically independent. This result is in line with Yu (2020). Figure 12 further presents that the correlation between NAOI and PVNUMI is  $-0.35$ , passing the 0.05 significance level. These results suggest that the summer NAO, as an independent potential driver which is unrelated to NAT, may also contribute to the summer TPSPV variation. This issue also deserves further study.

For the other climate factors controlling the summer TP, we calculated the concurrent correlation coefficient between the Niño3.4 index (SST averaged over  $5^{\circ}\text{S}$ – $5^{\circ}\text{N}$ ;  $170^{\circ}$ – $120^{\circ}\text{W}$ ; <https://psl.noaa.gov/data/climateindices/list/>) and PVNUMI and NATI during boreal summer. The results are  $-0.18$  and  $-0.17$ , which did not pass the significance test. This result means that the connection between NAT and TPSPV is linearly independent of ENSO.

Previous studies indicated that the spring NAT can last until the summer (Wu et al., 2009; Zheng et al., 2016); hence, the spring NAT can be regarded as a vital extratropical potential precursor to predict East Asian summer climate anomalies. Compared with ENSO, how and to what extent the NAT shapes the subsequent East Asian summer monsoon pattern deserves further investigation. In addition to the East Asian summer monsoon, the East Asian extreme events are prominently affected by the generation of TPSPV (Ma et al., 2019; Zhang et al., 2021). To what extent the NAT influences downstream extreme events by influencing the TPSPV is also worth further investigation. Clarifying these issues will help deepen our insight into the climate anomalies over East Asia.

## Data Availability Statement

All data sets used in this paper are publicly available. Three-hourly MERRA2 data archived at the hybrid  $\sigma$ - $p$  level (Global Modeling and Assimilation Office & Pawson, 2015a) are available at <https://doi.org/10.5067/WWQSXQ8IVFW8>. Monthly mean MERRA2 data archived at the pressure level (Global Modeling and Assimilation Office & Pawson, 2015c) are available at <https://doi.org/10.5067/2E096JV59PK7>. Monthly 2 m wind obtained from MERRA2 (Global Modeling and Assimilation Office & Pawson, 2015b) is available at <https://doi.org/10.5067/5ESKGQTZG7FO>. Monthly precipitation data from CRU (University of East Anglia Climatic Research Unit et al., 2019) are available at <https://doi.org/10.5285/10D3E3640F004C578403419AAC167D82>. The monthly COBE SST data set is available at <https://psl.noaa.gov/data/gridded/data.cobe.html>.

## References

- Bolin, B. (1950). On the influence of the Earth's orography on the general character of the westerlies. *Tellus*, 2(3), 184–195. <https://doi.org/10.3402/tellusa.v2i3.8547>
- Boos, W. R., & Kuang, Z. (2013). Sensitivity of the South Asian monsoon to elevated and non-elevated heating. *Scientific Reports*, 3, 1192. <https://doi.org/10.1038/srep01192>
- Charney, J. G., & Eliassen, A. (1949). A numerical method for predicting the perturbation of the middle latitude westerlies. *Tellus*, 1, 38–54. <https://doi.org/10.3402/tellusa.v1i2.8500>
- Chen, L. X., Liu, J. P., Zhou, X. J., & Wang, P. X. (1999). Impact of uplift of Qinghai–Xizang Plateau and change of land–ocean distribution on climate over Asia. *Acta Meteorologica Sinica*, 4, 314–329.
- Chiang, J. C. H., Kong, W., Wu, C. H., & Battisti, D. S. (2020). Origins of East Asian summer monsoon seasonality. *Journal of Climate*, 33(18), 7945–7965. <https://doi.org/10.1175/JCLI-D-19-0888.1>
- Cui, Y., Duan, A., Liu, Y., & Wu, G. (2015). Interannual variability of the spring atmospheric heat source over the Tibetan Plateau forced by the North Atlantic SSTA. *Climate Dynamics*, 45(5–6), 1617–1634. <https://doi.org/10.1007/s00382-014-2417-9>
- Deser, C., & Timlin, M. S. (1997). Atmosphere–ocean interaction on weekly timescales in the North Atlantic and Pacific. *Journal of Climate*, 10(3), 393–408. [https://doi.org/10.1175/1520-0442\(1997\)010<0393:A0IOWT>2.0.CO;2](https://doi.org/10.1175/1520-0442(1997)010<0393:A0IOWT>2.0.CO;2)
- Duan, A. M., Liu, Y. M., & Wu, G. X. (2005). Heating status of the Tibetan Plateau from April to June and rainfall and atmospheric circulation anomaly over East Asia in midsummer. *Science in China. Series D: Earth Sciences*, 48(2), 250–257. <https://doi.org/10.1360/02yd0510>
- Ertel, H. (1942). Ein neuer hydrodynamische wirbelsatz. *Meteorologische Zeitschrift Braunschweig*, 59, 33–49.
- Fallah, B., Cubasch, U., Proemmel, K., & Sodoudi, S. (2016). A numerical model study on the behaviour of Asian summer monsoon and AMOC due to orographic forcing of Tibetan Plateau. *Climate Dynamics*, 47(5–6), 1485–1495. <https://doi.org/10.1007/s00382-015-2914-5>

## Acknowledgments

This work is financially supported by the National Natural Science Foundation of China (41730963, 91837101, 42122035, and 91937302) and the Key Research Program of Frontier Sciences of the Chinese Academy of Sciences (XDB40030204 and XDB40030205). The authors thank the reviewers for their constructive and valuable suggestions and comments, which help us to substantially improve and strengthen the paper.

- Flohn, H. (1957). Large-scale aspects of the summer monsoon in South and East Asia. *Journal of the Meteorological Society of Japan*, 35A, 180–186. [https://doi.org/10.2151/jmsj1923.35a.0\\_180](https://doi.org/10.2151/jmsj1923.35a.0_180)
- Gelaro, R., McCarty, W., Suarez, M. J., Todling, R., Molod, A., Takacs, L., et al. (2017). The Modern-Era Retrospective analysis for Research and Applications, version 2 (MERRA-2). *Journal of Climate*, 30(14), 5419–5454. <https://doi.org/10.1175/JCLI-D-16-0758.1>
- Global Modeling and Assimilation Office, & Pawson, S. (2015a). MERRA-2 inst3\_3d\_asm\_Nv: 3d, 3-Hourly, Instantaneous, Model-Level, Assimilation, Assimilated Meteorological Fields V5.12.4. [Dataset]. <https://doi.org/10.5067/WWQSQXQ8IVFW8>
- Global Modeling and Assimilation Office, & Pawson, S. (2015b). MERRA-2 instM\_2d\_asm\_Nx: 2d, Monthly mean, Single-Level, Assimilation, Single-Level Diagnostics V5.12.4. [Dataset]. <https://doi.org/10.5067/5ESKGGQTZG7FO>
- Global Modeling and Assimilation Office, & Pawson, S. (2015c). MERRA-2 instM\_3d\_asm\_Np: 3d, Monthly mean, Instantaneous, Pressure-Level, Assimilation, Assimilated Meteorological Fields V5.12.4. [Dataset]. <https://doi.org/10.5067/2E096JV59PK7>
- He, B., Liu, Y. M., Wu, G. X., Wang, Z. Q., & Bao, Q. (2019). The role of air–sea interactions in regulating the thermal effect of the Tibetan–Iranian Plateau on the Asian summer monsoon. *Climate Dynamics*, 52(7–8), 4227–4245. <https://doi.org/10.1007/s00382-018-4377-y>
- He, B., Wu, G., Liu, Y., & Bao, Q. (2015). Astronomical and hydrological perspective of mountain impacts on the Asian summer monsoon. *Scientific Reports*, 5, 17586. <https://doi.org/10.1038/srep17586>
- Held, I. M., & Ting, M. (1990). Orographic versus thermal forcing of stationary waves—The importance of the mean low-level wind. *Journal of the Atmospheric Sciences*, 47(4), 495–500. [https://doi.org/10.1175/1520-0469\(1990\)047<0495:OVTFO>2.0.CO;2](https://doi.org/10.1175/1520-0469(1990)047<0495:OVTFO>2.0.CO;2)
- Held, I. M., Ting, M. F., & Wang, H. L. (2002). Orographic versus thermal forcing of stationary waves—The importance of the mean low-level wind. *Journal of Climate*, 15(16), 2125–2144. [https://doi.org/10.1175/1520-0442\(2002\)015<2125:NWSWTA>2.0.CO;2](https://doi.org/10.1175/1520-0442(2002)015<2125:NWSWTA>2.0.CO;2)
- Holton, J. R. (2004). *An introduction to dynamic meteorology*. Boston, MA: Elsevier.
- Hoskins, B., Pedder, M., & Jones, D. W. (2003). The omega equation and potential vorticity. *Quarterly Journal of the Royal Meteorological Society*, 129(595), 3277–3303. <https://doi.org/10.1256/qj.02.135>
- Hoskins, B. J. (1991). Towards a PV- $\theta$  view of the general-circulation. *Tellus Series A: Dynamic Meteorology and Oceanography*, 43(4), 27–35. <https://doi.org/10.1034/j.1600-0870.1991.t01-3-00005.x>
- Hoskins, B. J., & Ambrizzi, T. (1993). Rossby-wave propagation on a realistic longitudinally varying flow. *Journal of the Atmospheric Sciences*, 50(12), 1661–1671. [https://doi.org/10.1175/1520-0469\(1993\)050<1661:RWPOAR>2.0.CO;2](https://doi.org/10.1175/1520-0469(1993)050<1661:RWPOAR>2.0.CO;2)
- Hoskins, B. J., McIntyre, M. E., & Robertson, A. W. (1985). On the use and significance of isentropic potential vorticity maps. *Quarterly Journal of the Royal Meteorological Society*, 111(470), 877–946. <https://doi.org/10.1256/smsj.47001>
- Ishii, M., Shouji, A., Sugimoto, S., & Matsumoto, T. (2005). Objective analyses of sea-surface temperature and marine meteorological variables for the 20th century using ICOADS and the Kobe collection. *International Journal of Climatology*, 25(7), 865–879. <https://doi.org/10.1002/joc.1169>
- Jiang, D. B., Ding, Z. L., Drange, H., & Gao, Y. Q. (2008). Sensitivity of East Asian climate to the progressive uplift and expansion of the Tibetan Plateau under the mid-Pliocene boundary conditions. *Advances in Atmospheric Sciences*, 25(5), 709–722. <https://doi.org/10.1007/s00376-008-0709-x>
- Kim, B. J., Moon, S. E., & Lu, R. Y. (2002). Teleconnections: Summer monsoon over Korea and India. *Advances in Atmospheric Sciences*, 19(4), 665–676. <https://doi.org/10.1007/s00376-002-0006-z>
- Kitoh, A. (2004). Effects of mountain uplift on East Asian summer climate investigated by a coupled atmosphere–ocean GCM. *Journal of Climate*, 17(4), 783–802. [https://doi.org/10.1175/1520-0442\(2004\)017<0783:EOMUOE>2.0.CO;2](https://doi.org/10.1175/1520-0442(2004)017<0783:EOMUOE>2.0.CO;2)
- Kripalani, R. H., & Kulkarni, A. (2001). Monsoon rainfall variations and teleconnections over South and East Asia. *International Journal of Climatology*, 21(5), 603–616. <https://doi.org/10.1002/joc.625>
- Krishnan, R., & Sugi, M. (2001). Baiu rainfall variability and associated monsoon teleconnections. *Journal of the Meteorological Society of Japan*, 79(3), 851–860. <https://doi.org/10.2151/jmsj.79.851>
- Li, G., Chen, J., Wang, X., Luo, X., Yang, D., Zhou, W., et al. (2018). Remote impact of North Atlantic sea surface temperature on rainfall in southwestern China during boreal spring. *Climate Dynamics*, 50(1–2), 541–553. <https://doi.org/10.1007/s00382-017-3625-x>
- Li, Z. X., Yu, Y. Q., Deng, W. T., Zeng, G., & Wu, L. L. (2019). Variation characteristics of North Atlantic tri-polar sea surface temperature in spring and its relationship with NAO and ENSO (in Chinese). *Journal of the Meteorological Sciences*, 39, 721–730.
- Liang, H. Z., Wu, Q. G., Ren, X. J., Yao, Y. H., & Liu, S. Z. (2021). Impacts of decay of different El Niño types on boreal summer rainfall and surface air temperature in south Asian monsoon region and Tibetan Plateau (in Chinese). *Chinese Journal of Atmospheric Sciences*, 45, 777–798.
- Liu, X. D. (1999). Influences of Qinghai–Xizang (Tibet) Plateau uplift on the atmospheric circulation, global climate and environment changes (in Chinese). *Plateau Meteorology*, 18, 321–332.
- Liu, Y., Lu, M., Yang, H., Duan, A., He, B., Yang, S., & Wu, G. (2020). Land–atmosphere–ocean coupling associated with the Tibetan Plateau and its climate impacts. *National Science Review*, 7(3), 534–552. <https://doi.org/10.1093/nsr/nwaa011>
- Lu, M., Huang, B., Li, Z., Yang, S., & Wang, Z. (2019). Role of Atlantic air–sea interaction in modulating the effect of Tibetan Plateau heating on the upstream climate over Afro-Eurasia-Atlantic regions. *Climate Dynamics*, 53(1–2), 509–519. <https://doi.org/10.1007/s00382-018-4595-3>
- Lu, M., Yang, S., Li, Z., He, B., He, S., & Wang, Z. (2018). Possible effect of the Tibetan Plateau on the upstream climate over West Asia, North Africa, South Europe and the North Atlantic. *Climate Dynamics*, 51(4), 1485–1498. <https://doi.org/10.1007/s00382-017-3966-5>
- Lu, M. M., Yang, S., Wang, J. B., Wu, Y. T., & Jia, X. L. (2021). Response of regional Asian summer monsoons to the effect of reduced surface albedo in different Tibetan Plateau domains in idealized model experiments. *Journal of Climate*, 34(17), 7023–7036. <https://doi.org/10.1175/JCLI-D-20-0500.1>
- Ma, T. T., Wu, G. X., Liu, Y. M., Jiang, Z. H., & Yu, J. H. (2019). Impact of surface potential vorticity density forcing over the Tibetan Plateau on the South China extreme precipitation in January 2008. Part I: Data Analysis. *Journal of Meteorological Research*, 33(3), 400–415. <https://doi.org/10.1007/s13351-019-8604-1>
- Mitchell, T. D., & Jones, P. D. (2005). An improved method of constructing a database of monthly climate observations and associated high-resolution grids. *International Journal of Climatology*, 25(6), 693–712. <https://doi.org/10.1002/joc.1181>
- Nan, S. L., Zhao, P., & Chen, J. M. (2019). Variability of summertime Tibetan tropospheric temperature and associated precipitation anomalies over the central-eastern Sahel. *Climate Dynamics*, 52(3–4), 1819–1835. <https://doi.org/10.1007/s00382-018-4246-8>
- Neale, R. B., Richter, J., Park, S., Lauritzen, P. H., Vavrus, S. J., Rasch, P. J., & Zhang, M. (2013). The mean Climate of the Community Atmosphere Model (CAM4) in forced SST and fully coupled experiments. *Journal of Climate*, 26(14), 5150–5168. <https://doi.org/10.1175/JCLI-D-12-00236.1>
- Rienecker, M. M., Suarez, M. J., Gelaro, R., Todling, R., Bacmeister, J., Liu, E., et al. (2011). MERRA: NASA’s Modern-Era Retrospective analysis for Research and Applications. *Journal of Climate*, 24(14), 3624–3648. <https://doi.org/10.1175/JCLI-D-11-00015.1>
- Rosby, C. G. (1940). Planetary flow patterns in the atmosphere. *Quarterly Journal of the Royal Meteorological Society*, 66, 68–87.

- Sheng, C., He, B., Wu, G. X., Liu, Y. M., & Zhang, S. Y. (2022). Interannual influences of the surface potential vorticity forcing over the Tibetan Plateau on East Asian summer rainfall. *Advances in Atmospheric Sciences*. <https://doi.org/10.1007/s00376-021-1218-4>
- Sheng, C., Wu, G. X., Tang, Y. Q., He, B., Xie, Y. K., Ma, T. T., et al. (2021). Characteristics of the potential vorticity and its budget in the surface layer over the Tibetan Plateau. *International Journal of Climatology*, *41*, 439–455. <https://doi.org/10.1002/joc.6629>
- Son, J. H., Kwon, J. I., & Heo, K. Y. (2021). Weak upstream westerly wind attracts Western North Pacific typhoon tracks to west. *Environmental Research Letters*, *16*(12), 124041. <https://doi.org/10.1088/1748-9326/ac3aa4>
- Takaya, K., & Nakamura, H. (2001). A formulation of a phase-independent wave-activity flux for stationary and migratory quasi-geostrophic eddies on a zonally varying basic flow. *Journal of the Atmospheric Sciences*, *58*(6), 608–627. [https://doi.org/10.1175/1520-0469\(2001\)058<0608:AFOAPI>2.0.CO;2](https://doi.org/10.1175/1520-0469(2001)058<0608:AFOAPI>2.0.CO;2)
- Tao, Y. W., Sun, Z. B., Li, W. J., Li, W. P., & Zuo, J. Q. (2011). Relationships between ENSO and Qinghai–Tibetan Plateau snow depth and their influences on summer rainfall anomalies in China (in Chinese). *Meteorological Monthly*, *37*, 919–928.
- University of East Anglia Climatic Research Unit (CRU), Harris, I. C., & Jones, P. D. (2019). CRU TS4.03: Climatic Research Unit (CRU) Time-Series (TS) version 4.03 of high-resolution gridded data of month-by-month variation in climate (Jan. 1901–Dec. 2018). [Dataset]. Centre for Environmental Data Analysis (CEDA). <https://doi.org/10.5285/10D3E3640F004C578403419AAC167D82>
- Wang, B., Wu, R., & Lau, K. M. (2001). Interannual variability of the Asian summer monsoon: Contrasts between the Indian and the Western North Pacific–East Asian monsoons. *Journal of Climate*, *14*(20), 4073–4090. [https://doi.org/10.1175/1520-0442\(2001\)014<4073:IVOTAS>2.0.CO;2](https://doi.org/10.1175/1520-0442(2001)014<4073:IVOTAS>2.0.CO;2)
- Watanabe, M., & Kimoto, M. (2000). Atmosphere–ocean thermal coupling in the North Atlantic: A positive feedback. *Quarterly Journal of the Royal Meteorological Society*, *126*(570), 3343–3369. <https://doi.org/10.1002/qj.49712657017>
- Watanabe, M., Kimoto, M., Nitta, T., & Kachi, M. (1999). A comparison of decadal climate oscillations in the North Atlantic detected in observations and a coupled GCM. *Journal of Climate*, *12*(9), 2920–2940. [https://doi.org/10.1175/1520-0442\(1999\)012<2920:ACODCO>2.0.CO;2](https://doi.org/10.1175/1520-0442(1999)012<2920:ACODCO>2.0.CO;2)
- Wen, Q., & Yang, H. (2020). Investigating the role of the Tibetan Plateau in the formation of Pacific meridional overturning circulation. *Journal of Climate*, *33*(9), 3603–3617. <https://doi.org/10.1175/JCLI-D-19-0206.1>
- Wu, G., Zhuo, H., Wang, Z., & Liu, Y. (2016). Two types of summertime heating over the Asian large-scale orography and excitation of potential-vorticity forcing I. Over Tibetan Plateau. *Science China Earth Sciences*, *59*(10), 1996–2008. <https://doi.org/10.1007/s11430-016-5328-2>
- Wu, G. X., Li, W. J., & Guo, H. (1997). Sensible heat driven air-pump over the Tibetan Plateau and its impacts on the Asian summer monsoon. In D. Z. Ye (Ed.), *Collection in memory of Zhao Jiuzhang* (pp. 116–126). Beijing, China: Science Press.
- Wu, G. X., Liu, Y. M., He, B., Bao, Q., Duan, A. M., & Jin, F. F. (2012). Thermal controls on the Asian summer monsoon. *Scientific Reports*, *2*, 1–7. <https://doi.org/10.1038/srep00404>
- Wu, G. X., Liu, Y. M., Wang, T. M., Wan, R. J., Liu, X., Li, W. P., et al. (2007). The influence of mechanical and thermal forcing by the Tibetan Plateau on Asian climate. *Journal of Hydrometeorology*, *8*(4), 770–789. <https://doi.org/10.1175/jhm609.1>
- Wu, R. (2002). A mid-latitude Asian circulation pattern in boreal summer and its connection with the Indian and East Asian summer monsoons. *International Journal of Climatology*, *22*(15), 1879–1895. <https://doi.org/10.1002/joc.845>
- Wu, R. (2017). Relationship between Indian and East Asian summer rainfall variations. *Advances in Atmospheric Sciences*, *34*(1), 4–15. <https://doi.org/10.1007/s00376-016-6216-6>
- Wu, Z. W., Wang, B., Li, J. P., & Jin, F. F. (2009). An empirical seasonal prediction model of the east Asian summer monsoon using ENSO and NAO. *Journal of Geophysical Research: Atmospheres*, *114*, D18120. <https://doi.org/10.1029/2009jd011733>
- Xu, X. Y., & Wang, Y. F. (2016). Analysis of the influence of ENSO on snow depth over Qinghai–Xizang Plateau and its continuity (in Chinese). *Plateau Meteorology*, *35*, 1–12.
- Yanai, M. H., Li, C. F., & Song, Z. S. (1992). Seasonal heating of the Tibetan Plateau and its effects on the evolution of the Asian summer monsoon. *Journal of the Meteorological Society of Japan*, *70*(1B), 319–351. [https://doi.org/10.2151/jmsj1965.70.1B\\_319](https://doi.org/10.2151/jmsj1965.70.1B_319)
- Yang, H., & Wen, Q. (2020). Investigating the role of the Tibetan Plateau in the formation of Atlantic Meridional Overturning Circulation. *Journal of Climate*, *33*(9), 3585–3601. <https://doi.org/10.1175/JCLI-D-19-0205.1>
- Ye, D. Z., & Gao, Y. X. (1979). *The meteorology of the Qinghai–Xizang (Tibet) Plateau*. Beijing, China: Science Press.
- Ye, D. Z., Luo, S. W., & Zhu, B. Z. (1957). The wind structure and heat balance in the lower troposphere over Tibetan Plateau and its surroundings (in Chinese). *Acta Meteorologica Sinica*, *28*, 108–121. <https://doi.org/10.11676/qxxb1957.010>
- Yu, J. H., Liu, Y. M., Ma, T. T., & Wu, G. X. (2019). Impact of surface potential vorticity density forcing over the Tibetan Plateau on the South China extreme precipitation in January 2008. Part II: Numerical Simulation. *Journal of Meteorological Research*, *33*(3), 416–432. <https://doi.org/10.1007/s13351-019-8606-z>
- Yu, W., Liu, Y., Yang, X.-Q., Wu, G., He, B., Li, J., & Bao, Q. (2021). Impact of North Atlantic SST and Tibetan Plateau forcing on seasonal transition of springtime South Asian monsoon circulation. *Climate Dynamics*, *56*(1–2), 559–579. <https://doi.org/10.1007/s00382-020-05491-0>
- Yu, Y. Q. (2020). *The North Atlantic sea surface temperature tripole in all seasons and its relationship with interannual variability of temperature in China* (Master's thesis in Chinese). Nanjing, China: Nanjing University of Information Science and Technology. Retrieved from China National Knowledge Infrastructure ([https://kns.cnki.net/kcms/detail/detail.aspx?dbcode=CMFD&dbname=CMFD202101&filename=1021505070.nh&uniplatform=NZKPT&v=mnMCGG\\_BSSpABXqSo6CWIHkukTIq8\\_omtfmkFpP\\_Xx-u08Q-C6D8mqRMRpiVpHU6](https://kns.cnki.net/kcms/detail/detail.aspx?dbcode=CMFD&dbname=CMFD202101&filename=1021505070.nh&uniplatform=NZKPT&v=mnMCGG_BSSpABXqSo6CWIHkukTIq8_omtfmkFpP_Xx-u08Q-C6D8mqRMRpiVpHU6))
- Zhang, G., Mao, J., Liu, Y., & Wu, G. (2021). PV perspective of impacts on downstream extreme rainfall event of a Tibetan Plateau Vortex collaborating with a Southwest China Vortex. *Advances in Atmospheric Sciences*, *38*(11), 1835–1851. <https://doi.org/10.1007/s00376-021-1027-9>
- Zhao, G., Huang, G., Wu, R., Tao, W., Gong, H., Qu, X., & Hu, K. (2015). A new upper-level circulation index for the East Asian summer monsoon variability. *Journal of Climate*, *28*(24), 9977–9996. <https://doi.org/10.1175/JCLI-D-15-0272.1>
- Zhao, P., & Chen, L. X. (2001). Climate features of atmospheric heat source/sink over the Qinghai–Xizang Plateau in 35 years and its relation to rainfall in China. *Science in China. Series D: Earth Sciences*, *44D*, 858–864. <https://doi.org/10.1007/bf02907098>
- Zhao, Y., Duan, A., & Wu, G. (2018). Interannual variability of late-spring circulation and diabatic heating over the Tibetan Plateau associated with Indian Ocean forcing. *Advances in Atmospheric Sciences*, *35*(8), 927–941. <https://doi.org/10.1007/s00376-018-7217-4>
- Zheng, F., Li, J., Li, Y., Zhao, S., & Deng, D. (2016). Influence of the summer NAO on the spring-NAO-based predictability of the East Asian summer monsoon. *Journal of Applied Meteorology and Climatology*, *55*(7), 1459–1476. <https://doi.org/10.1175/jamc-d-15-0199.1>